UNDERSTANDING THE PERFORMANCE OF A PROGRESSIVE CAVITY PUMP WITH A METALLIC STATOR

by

Jose Gamboa

Research Engineer

Aurelio Olivet

Production Engineer

Juan Iglesias

Researcher

and

Pedro Gonzalez

Researcher

Research and Development Institute

Petróleos de Venezuela, S.A. (PDVSA-Intevep)

Los Teques, Venezuela

Jose Gamboa is a Research Engineer with the Research and Development Institute of Petróleos de Venezuela, S.A. (PDVSA-Intevep), at Los Teques, Venezuela. He works as an artificial lift specialist and researcher in laboratory studies of progressing cavity pumps as applied to crude oil production.

Mr. Gamboa obtained his diploma (Mechanical Engineering, 1994) from the Universidad Metropolitana. He received his Masters degree (Mechanical Engineering, 2000) from the Universidad Simon Bolivar.

Aurelio Olivet is a Production Engineer with the Research and Development Institute of Petróleos de Venezuela, S.A. (PDVSA-Intevep), at Los Teques, Venezuela. He obtained his Bachelor's degree (Chemical Engineering, 1998) from the Universidad Simon Bolivar. He studied the two-phase performance of a progressing cavity pump with a metallic stator for his Master's thesis and received his Master's degree (Mechanical Engineering, 2002) from the Universidad Simon Bolivar.

Juan Iglesias is a Researcher with the Research and Development Institute of Petróleos de Venezuela, S.A. (PDVSA-Intevep), at Los Teques, Venezuela. Since 1993, he has worked as a specialist in the artificial lift method and has done research in pumping systems for the production of crude oil.

ABSTRACT

Analytical and experimental studies were carried out on a progressive cavity pump (PCP) fitted with a metallic stator with a fixed, positive clearance around the single helical rotor. This eliminates wear and greatly increases pump life, but it allows leakage or slip back to suction, which decreases the net output flow rate for a given imposed pressure rise. On the other hand, conventional PCPs have an elastomeric stator surrounding the rotor at zero clearance, so there is zero leakage until this stator wears out.

Computations made on three analytical models provided insight into the internal leakage of this new type of PCP and pointed the way for further more definitive performance analysis in the future. These models, which utilized computational fluid dynamics (CFD), were:

- Flow past a rotating cylinder between two closely fitted parallel plates,
- Flow past a straight wall with a developed ("untwisted") stator flute moving axially along this wall—like a convergent-divergent bearing space that has wedge flow and the associated developed positive and negative pressures, and
- Flow through a slit that models the clearance between the rotor and the surrounding stator (called the "model of the PCP").

Experiments were conducted under single-phase and two-phase conditions in order to acquire performance data for an actual PCP with a metallic stator. Pressure sensors installed inside the pump measured instantaneous cavity pressures and enabled comparison of these measurements with the CFD simulations. Liquid viscosity in the single-phase tests varied from 1 to 480 cP. Light oil with a viscosity of 42 cP was used for the multiphase tests, in which the intake gas void fraction was varied from zero to 80 percent. The test pump had a 40 mm (1.58 inches) rotor and was run over a speed range from 100 to 1200 rpm.

The performance curves obtained from the experiments form a valuable database for users who would be interested in applying this new PCP pump type. More significantly, these results validate the use of PCPs with metallic stators in the production of heavy and extra-heavy crude oil.

INTRODUCTION

Heavy and extra-heavy crude oil production is characterized by the handling of fluid of very high viscosity (greater than 300 cP at 150°F), high gas void fraction (GVF) (greater than 40 percent), and mixtures of crude oil, gas, water, and sand. Therefore, the production costs of this crude oil are greater than the costs of producing light and medium crude oil. Additionally, the new techniques of production with steam injection add the problem of handling fluid with temperatures above 300°F.

In contrast the sale price is approximately 30 percent less than light and medium crude. Therefore, the challenge in producing heavy and extra-heavy crude oil is to achieve a profitable improvement in the process of extraction (Figure 1). This implies a higher efficiency of the extraction system that allows the reduction of energy consumption, an increase in production volume, diminished costs due to replacement of equipment, and extended operating life of equipment used for subsurface extraction.

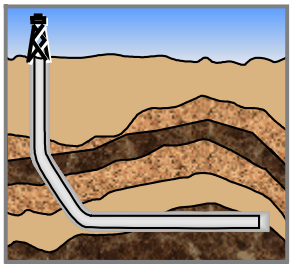

Figure 1. Representation of Heavy and Extra-Heavy Crude Oil Extraction Process.

The progressing cavity pump (PCP) (Figure 2) is one of the three pumping systems used in extraction of highly viscous crude oil. The PCP has been the pumping system most widely used in this application, since these pumps have demonstrated higher mechanical efficiency than rotordynamic pumping systems (called electro-submergible pumps—ESPs) together with lower initial investment and energy consumption. Besides, the PCP can handle sand and greater GVF than the reciprocating pumping system known as the "sucker rod pumping system."

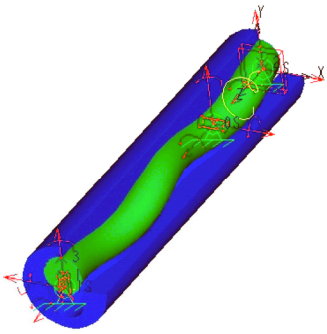

Figure 2. Representation of Progressing Cavity Pump.

Nevertheless, extensive use of PCPs has been limited, because factors such as the temperature of fluids handled, chemical incompatibility with gases and liquid produced, and the high differential pressure applied to pumps during operation affects their running life and reduces their volumetric and mechanical efficiency, resulting in increased operational cost.

As illustrated in Cooper, et al. (2001), a PCP is a screw pump with a single, helical rotor. More detail can be found in Cholet (1997) and in Dunn, et al. (1994). Traditionally, PCPs have been fitted with elastomeric stators that allow them to operate with zero internal clearance. While this eliminates internal leakage or slip, the achievable pressure rise and life have been limited. Related performance information can be found in Arrellano (1998). Net positive suction head (NPSH) performance has been addressed by Dillon and Vullings (1999) and studied by Vetter and Paluchowski (1997). Some researchers such as Pardey (1999) have proposed replacing the elastomeric material used for the stator with other material having better mechanical properties, higher chemical resistance, and tolerance to elevated temperature. But, according to Moineau's rule, contact must exist between rotor and stator for successful operation of the pump. Under this rule, only materials with very low friction coefficient could be used for the stator.

Vetter and Wirth (1995) found that this is not necessarily true, and they demonstrated that a progressing cavity pump with clearance between rotor and stator could work. This makes possible the use of metallic material, such as steel, bronze, and alloy. Any of these materials could be specified, but the question would be the performance of a pump with such a material.

Therefore, the following research has as its objective the study of the performance of a progressing cavity pump with a metallic stator. Further, results obtained via computational fluid simulation have been compared with experiments made in bench testing of a PCP with a steel stator. The goal is to understand the physical phenomena governing the pump performance and to evaluate the application of this new PCP to the production of crude oil.

Understanding conventional PCPs through numerical simulation has been reported by Osio and Moreno (1996). In an attempt to simulate the PCP with a metallic stator, three models were utilized to analyze the performance of this pump via finite element analysis (refer to Gamboa, 2000, and Olivet, 2002). The first model was called the "infinite parallel plate." It was proposed by Belcher (1991) and simulates the slippage effect as that of a convergent-divergent bearing. The second model was called the "untwisted model." It was proposed by Robles (1995) and is an equivalent model of operation of a PCP. Finally, all steps in the construction of a real model of a one-stage PCP are explained, emphasizing the problems found in trying to simulate the hydrodynamics of the pump. Incompressible, Newtonian fluids were assumed under isothermal conditions in a pump twice the size of the test pump.

Originally the experiments were designed to produce data that would validate the results of the CFD simulations. However, these simulations have not provided sufficient knowledge about the behavior of this machine. For this reason, it was decided to conduct single-phase and two-phase experiments so as to better understand the pump's performance. Multiphase testing was done for conventional PCPs by Martin, et al. (1999), and Martín (1999) described multiphase flow behavior in these pumps.

Single-phase experiments were conducted with water and three lube oils at rotational speeds from 100 to 1200 rpm, while experiments under two-phase conditions were made at speeds from 100 to 400 rpm with a liquid viscosity of 42 cP and GVF of 20, 50, and 80 percent. Additionally, pressure sensors were installed inside the pump for measuring the instantaneous pressure in the cavity. These measurements were compared with CFD simulations.

The results indicated that Couette flow (Schlichting, 1986) exists between rotor and stator at zero differential pressure. But if differential pressure increases, a reverse slip flow called Poiseuille flow reduces the total volume displaced. This reverse flow creates regions of high pressure that create a seal between adjacent cavities.

The experimental results include the effects of angular velocity, viscosity, and gas void fraction on pump performance. It was found that a PCP with a metallic stator is a multiphase pump.

Finally, the experimental results confirm that PCPs with metallic stators can be used in production crude oil of high viscosity (above 40 cP).

BASIC KNOWLEDGE

R. Moineau (1930) defined all basic parameters and concepts that characterize the performance of progressing cavity pumps. These parameters and concepts were derived on the basis of contact between rotor and stator. However, G. Vetter (Vetter and Wirth, 1995) found divergence between these concepts and his experimental results. He proposed this divergence was because the concepts defined by Moineau did not include the parameter known as "interference." The interference, w, is the algebraic difference between the radii of rotor and stator (Equation (1)).

$$w = \frac{d_r - d_{st}}{2} \tag{1}$$

According to the value of w, a PCP can be classified as (Figure 3):

- A pump with positive interference, when the radius of the rotor is bigger than the radius of the stator, producing contact between both elements and creating deformation in the stator.
- A pump with zero interference, when rotor and stator have the same dimensions and point contact exists between both elements.

• A pump with negative interference, when the stator radius stator is bigger than the rotor radius rotor, creating a clearance between both components.

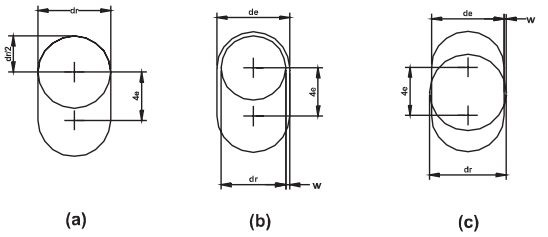

Figure 3. Classification of PC Pump According to Value of Interference.

Previous work (Vetter and Wirth, 1995, and Gómez, 2000) demonstrated that the traditional concept proposed by Moineau could induce errors in calculating volumetric efficiency and hydraulic power. Therefore, properties such as displacement, theoretical flow rate, and kinematics are now analyzed.

The displacement of a PCP with negative interference can be calculated beginning with the free volume between rotor and stator. This free volume can be obtained by multiplying the free area of a cross section of pump by the stator pitch. The free area for a PCP with negative interference is given by Equation (2):

$$A = 4ed_r - 8ew - \pi\left(d_r w - w^2\right) \tag{2}$$

In this manner, the free volume is obtained from Equation (3):

$$D = \left(4ed_r - 8ew - \pi\left(d_r w - w^2\right)\right) * Pitch_{st} \tag{3}$$

Then, the theoretical flow rate can be calculated by multiplying the displacement by the rotational speed (Equation (4)):

$$Q_t = \left(4ed_r - 8ew - \pi\left(d_r w - w^2\right)\right) * Pitch_{st} * n_{rotor} \tag{4}$$

Another property that changes radically is the kinematic principle of pump operation. In a pump with positive or zero interference, the kinematics of the rotor are a consequence of contact between it and the stator. This contact limits the degree of freedom of movement of the rotor, causing it to describe only a movement known as a hypocycloid as it rotates. In the case of a PCP with negative interference, contact does not exist between rotor and stator, the rotor has an additional degree of freedom that allows it to rotate and displace in two directions so as to describe an ellipsoidal movement (Figure 4).

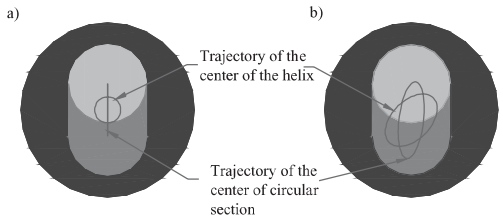

Figure 4. Rotor Trajectory. (a) Hypocycloidal Movement, (b) Ellipsoidal Movement.

However, the presence of fluid inside the pump further affects the kinematics of the rotor. If the fluid handled is incompressible, during operation the fluid fills the clearance between rotor and stator. Then it produces an effect similar to a convergent-divergent bearing observed and proposed in previous studies (Belcher, 1991). This hydrodynamic effect prevents the rotor from contacting the wall of the stator, restricting its movement and obligating it to describe a hypocycloidal movement.

COMPUTATIONAL FLUID SIMULATION OF PROGRESSIVE CAVITY PUMPS

Modeling

Simulating the hydraulic behavior of a progressing cavity pump is a transitory flow problem, with irregular and nonsymmetric geometry. Moreover, with existing techniques of simulation this is a difficult problem to solve.

The strategy for solving this problem began from a simple model that increased in complexity in the attempt to achieve successful simulation of a PCP. The scope was to understand the basic principle of operation of the pump, the mechanism of creating a seal, and the effect of slippage between cavities.

Three models were created:

• Model #1 was called the "infinite parallel plate," which attempts to simulate the hydrodynamic bearing effect that is created between the rotor and the stator during pump operation;

• Model #2 is known as the "developed model" or the "untwisted model," which is an equivalent model of the pump that provides an understanding of its operation; and

• Model #3 is a full model of one stage of a PCP.

These models will be explained in depth in later sections, nevertheless it is important to indicate that for all the cases the following conditions were assumed:

• Fluid flow was strictly laminar;

• Fluid was considered as Newtonian, single-phase, and incompressible; and

• The temperature is constant for the entire simulation.

The simulation of a PCP is a problem with a time-varying border whose domain must be determined according to the position of the rotor inside the pump. Thus, the simulation code used must offer the options of a variable border and readjustment of meshes. Only codes that are based on finite element techniques (e.g., refer to Huebner and Thornton, 1982) offer such options; therefore, all simulations were made using a finite element flow modeling (CFD) software tool. A commercially available preprocessor was used for creating the mesh and geometry. All packages were executed on a workstation operating under a UNIX® operating system with 256 MB of random access memory (RAM) and a 40 GB hard disk.

The strategy followed for the creation of the models was to create the geometry in a computer aided drawing (CAD) package and export it to the software that generates the mesh. Subsequently the mesh was created within the fluid space, and the quality of the mesh was measured by means of a "distortion index." Finally, the created model was imported into the CFD software. Here the boundary conditions, element types, and other specifications were defined, and the problem was solved for each case.

Model #1—Infinite Parallel Plate

Belcher (1991) proposed to approximate the slippage inside a PCP by that through a convergent-divergent bearing. This means that slippage in the pump can be approximated as flow between two parallel plates of infinite length, which are separated by a distance equal to the diameter of the stator. Between them rotates a cylinder (also of infinite length) of the same diameter as the rotor (Figure 5).

The plates were denoted as the upper and lower limits of the domain, whereas the ports to the right and left of the model were called the entrance and exit limits. The cylinder was called the rotor (Figure 6).

The boundary conditions were specified as follows:

• The fluid velocity near the wall is equal to zero,

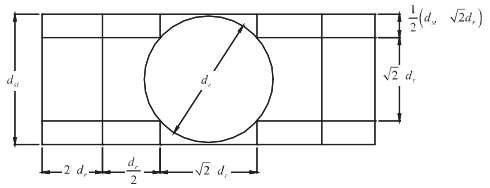

Figure 5. Representation of "Infinite Parallel Plate" Model.

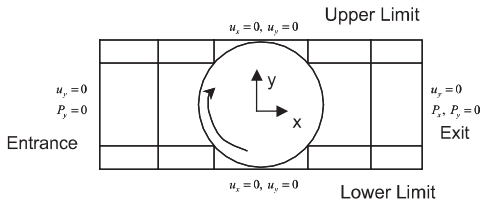

Figure 6. Limits of Computational Domain.

- The vector of liquid velocity is normal to the area in the entrance and exit ports, and
- The angular velocity of the rotor was simulated as tangential velocity at the periphery of the rotor, as calculated from Equation (5).

$$U_T = \frac{\pi}{60} \cdot n \cdot d_r \tag{5}$$

The fluid in this domain was divided into 14 regions. The mesh was created starting with quadrilateral elements that resulted in a mesh with 12,496 nodes (Figure 7).

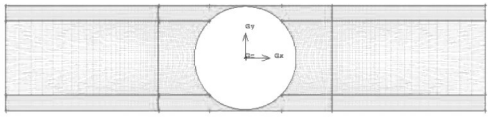

Figure 7. Mesh Created for Model #1.

Model #2—2D Developed or "Untwisted" Model

Robles (1986) modeled the operation of a progressing cavity pump starting with an equivalent model called the "untwisted model." It consists of unrolling (developing) the stator of the pump, holding the faces of the stator parallel, while the rotor is created starting with Equation (6).

$$\begin{aligned}\vec{h} = \Bigg\{ & \left[\left| \vec{R}_1 \right| \sin(\phi_{st} - \alpha_{st}) - 2e\cos(2\alpha_{st}) - \frac{d_r}{2}\sin(\phi_r - 2\alpha_{st}) \right] \\ & + \left[-\left| \vec{R}_1 \right| \cos(\phi_{st} - \alpha_{st}) - \frac{d_r}{2}\cos(\phi_r - 2\alpha_{st}) \right] \Bigg\} \cdot \hat{j} \\ & + \frac{Paso_{st}}{2\pi}\alpha_{st} \cdot \hat{k} \Bigg|\end{aligned} \tag{6}$$

In this model the shape of the rotor results in the formation of cavities, and for this reason the lengths of the cavities must be equal to the pitch of the stator (Figure 8).

Generally, the rotor in a PCP describes a hypocycloid movement. In the untwisted model the rotor must move axially, in order for the volume displaced to equal that of the real model. Therefore, two conditions must be fulfilled:

- Both rotor and stator of the equivalent model are of infinite length, and
- The axial velocity of the rotor in the equivalent model is given by Equation (7).

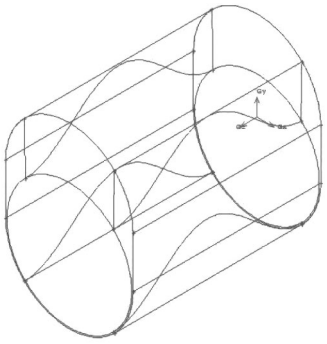

Figure 8. Representation of "Untwisted Model."

$$U_N = \frac{Pitch_{st} \cdot n}{60} \tag{7}$$

Using this model, two cases of study can be considered. For the first case, it is assumed that there is symmetry between the cavities, allowing division of the untwisted model into two sections of the pump that work in parallel. Thus, a two-dimensional model can be created (Figure 9). The second case is the study of a full three-dimensional model (Figure 10). This paper concentrates on the two-dimensional case, leaving for future work the analysis of the three-dimensional model.

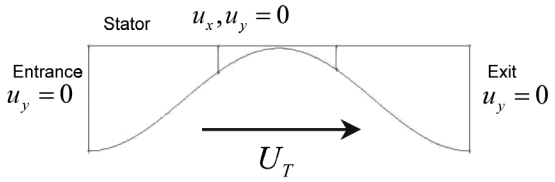

Figure 9. 2D Representation of Untwisted Model.

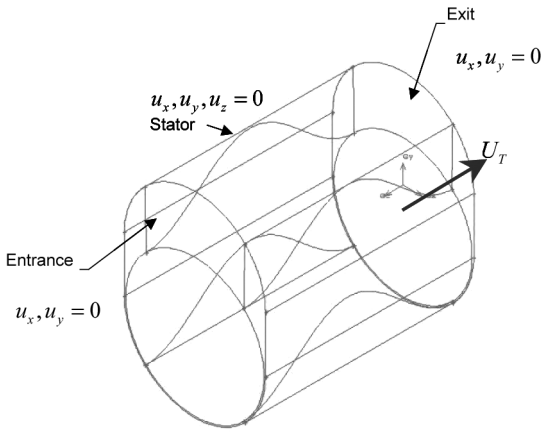

Figure 10. Full 3D Representation of Untwisted Model.

The two-dimensional model was created from the dimensions given in Table 1. For meshing, the domain was divided in three regions (Figure 11), which were meshed using quadrilateral elements with four nodes per element. A total of 422 elements was used with a distortion index of 8 percent.

Table 1. Geometric Parameters.

Interference (mm)	-0.370
Rotor diameter (mm)	39.878
Eccentricity (mm)	4.039
Stator Pitch (mm)	119.990

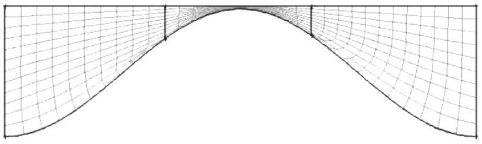

Figure 11. Meshing of Two-Dimensional Untwisted Model.

For the boundary conditions it was assumed that the fluid velocity in the x-direction is zero near the rotor, whereas on the stator it was assumed that all the components of the velocity vector were equal to zero.

Model #3—Progressing Cavity Pump

In order to create the full model of the PCP it was necessary to develop subroutines in Fortran for generating a path of the motion of the model. The step-by-step procedure can be described as follows:

- With a CAD package, the geometry was created and dimensions confirmed.
- Surfaces created with the CAD package were exported to the meshing package where both elements were converted into solid models.
- The solid model of the rotor was removed from that of the stator, thereby creating the fluid region.
- The fluid region was meshed using tetrahedral elements of four nodes per element (Figure 12).

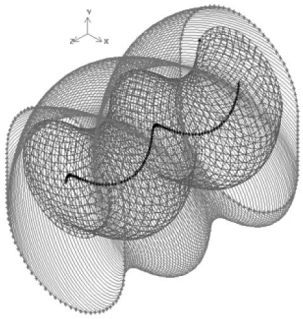

Figure 12. Representation of One Stage of PCP.

The mesh using tetrahedral elements did not allow completion of the meshing process. Distortions occurred in the internal element producing the mesh causing the procedure to be aborted. This problem was created by the difference between the helix angles of rotor and stator. Although different techniques were proven to create meshing of this domain, it could not be accomplished for the chosen geometry (Table 1).

At this point the option was trying to model a slit of the pump and thus to avoid the effect of distortion arising from the difference between the helices. This slit was long enough so that the helix angle of the stator was smaller than 10 degrees. Thus, the geometry of the pump was reduced to the model presented in Figure 13.

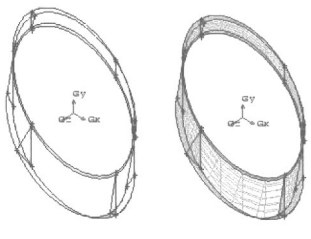

Figure 13. Model of Slit Formed Within PCP. (a) Model, (b) Mesh.

For the boundary conditions:

- In the entrance, it was assumed that velocity vectors of fluid are perpendicular to the normal vector of the cross sectional area, and
- At the stator wall, the vector velocity of the fluid was assumed to be zero (Figure 14).

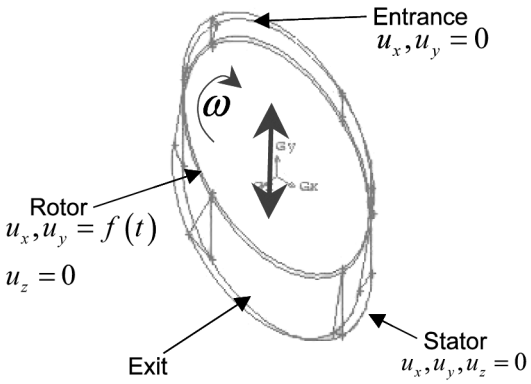

Figure 14. Boundary Conditions for Model #3.

SIMULATIONS

Model #1—Infinite Parallel Plate

The first case to simulate was the rotating cylinder when the difference of pressure between both ports is equal to zero. The simulation was made for a fluid viscosity of 133 cP.

In Figure 15 it is observed that the fluid near the cylinder (rotor) moves with and equals its peripheral velocity. Then the liquid is forced to circulate through the clearances between the rotor and the plates.

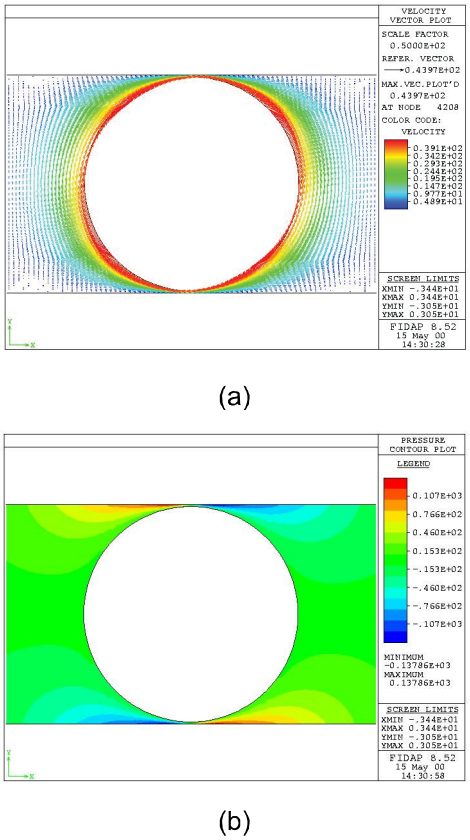

Figure 15. Results of "Infinite Parallel Plate" Simulation at 300 RPM and Viscosity of 133 CP. (a) Vector Velocity Distribution, (b) Pressure Distribution.

As the angular velocity of the cylinder increases, the pressure in the clearances rises with the average speed in this region. As a consequence, the fluid is accelerated and decelerated, forming regions of high and low pressure. The resulting gradient of pressure promotes the circulation of liquid in the direction of rotation of the rotor.

The second case studied was applying a gradient of pressure between the entrance and exit ports to the model of the rotating cylinder. This gradient was created by increasing the pressure in the entrance port. The difference of pressure between both ports induces a flow from the entrance port toward the exit port. This flow divides at the rotor and tries to circulate through the clearances.

In Figure 16 it is observed that flow induced by differential pressure tries to flow through the lower clearance, opposing the flow produced by the rotation of the cylinder. So the average velocity of the liquid in this region is reduced. The opposite effect occurs in the upper clearance, increasing the average velocity of the liquid. Therefore, a region of low flow or stagnation is created in the lower clearance, and another region of high flow is present in the upper clearance. If the differential pressure between both ports is increased sufficiently, the flow in the upper clearance becomes great enough to form a region of recirculation that opposes the flow of the fluid toward the exit port (Figure 17).

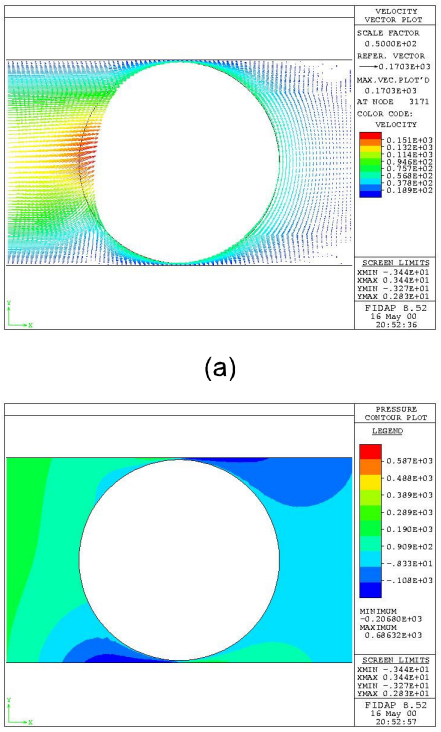

Figure 16. "Infinite Parallel Plate" Simulation at 300 RPM, Differential Pressure of 689 Dynes/CM^2 (= 68.9 PA or 0.01 PSI), and Liquid Viscosity of 133 CP. (a) Vector Velocity Distribution, (b) Pressure Distribution.

These results indicate the sealing inside a PCP without interference has as much to do with the rotation of the rotor as with the differential pressure between the cavities. Further, this indicates that the hydraulic mechanism of sealing in a PCP must be understood in terms of the zones of concurrence and recirculation of flow in the clearances between the rotor and the stator.

Model #2—2D Untwisted (Developed) Model

Figure 18 shows velocity profiles and the pressure distribution for the two-dimensional untwisted (developed) model, assuming

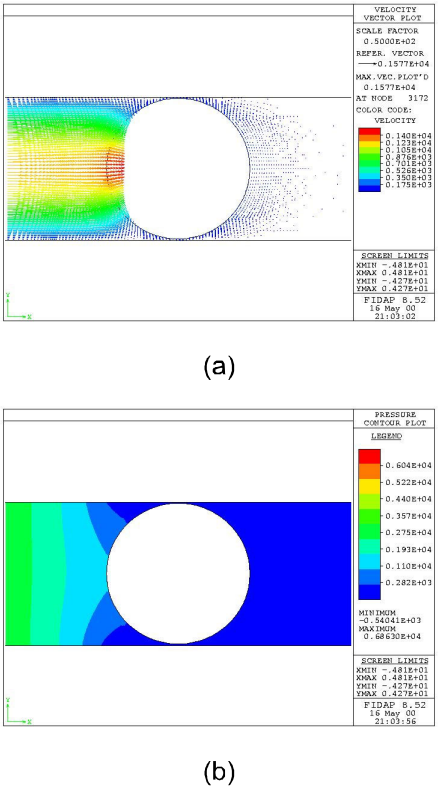

Figure 17. "Infinite Parallel Plate" Simulation at 300 RPM, Differential Pressure of 6849 Dynes/CM^2 (= 684.9 PA or 0.1 PSI), and Liquid Viscosity of 133 CP. (a) Vector Velocity Distribution, (b) Pressure Distribution.

that the fluid is Newtonian and has a viscosity of 133 cP, for an axial velocity of 1 cm/s (.033 ft/s). The differential pressure between the entrance and exit ports was equal to zero. Figure 18 shows that the moving rotor displaces all fluid inside the pump without increasing the pressure.

This result demonstrates that the pump operates in a manner similar to the relative movement of parallel plates, creating Couette flow. So the fluid moves axially without generating an increase of pressure, as with all positive displacement pumps.

The increase of pressure in the discharge port produces a migration of fluid from this zone toward the cavity opened to discharge. This migration of fluid causes elevation of pressure in the cavity exposed, demonstrating that the pump reacts to the pressure, never generates it. Then the rotor must push the fluid until it has been expelled.

The cavity open to discharge takes on the pressure of the discharge port, creating a difference of pressure with respect to its adjacent cavity. This differential pressure produces leakage of the fluid between both cavities, which is understood as slip. The slip creates a region where the flow is a combination of that caused by the displacement of the rotor and that produced by the pressure difference.

In this region the average velocity of the fluid is reduced with respect to velocity of fluid in the cavity. It produces a reduction in net volume displaced. Regions of high and low pressure near clearance regions were observed, indicating the preferential direction of the flow (Figure 19).

The obtained results of the untwisted model demonstrate that the slippage between the cavities must be understood as a zone of stagnation where the relative velocity of the fluid with respect to rotor is reduced.

Model #3—Progressing Cavity Pump

In Figure 20 the results are presented for simulating the PCP as a slit. This was done for a fluid whose viscosity was equal to 133 cP.

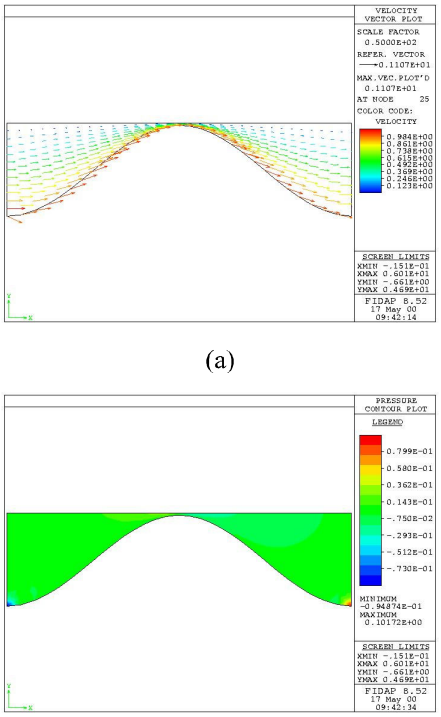

Figure 18. Results of 2D Untwisted Model Simulation for Tangential Velocity of 30 CM/S, Liquid Viscosity of 133 CP, and Zero Discharge Pressure. (a) Vector Velocity Distribution, (b) Distribution of Pressure.

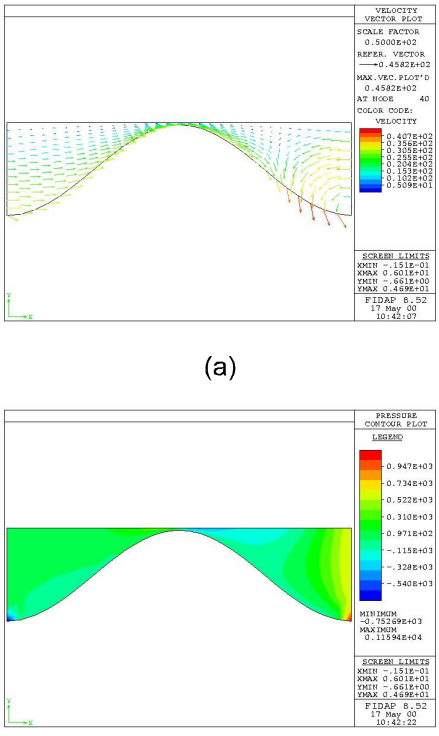

Figure 19. Results of 2D Untwisted Model Simulation for Tangential Velocity of 30 CM/S, Liquid Viscosity of Liquid of 133 CP, and Discharge Pressure of 6.98 PA (= 0.001 PSI). (a) Vector Velocity Distribution, (b) Distribution of Pressure.

This result demonstrated that maximum velocity of the fluid is reached over the greater portion of the cross-sectional area of the cavity. However, the small number of elements prevented better results from being obtained.

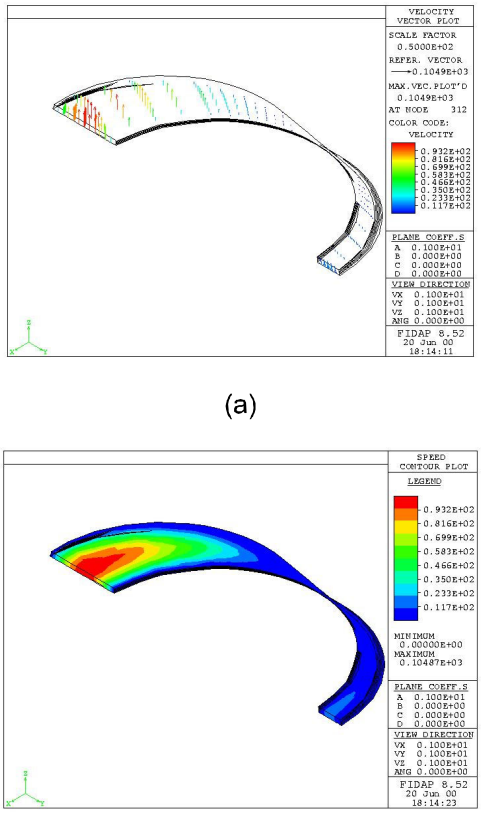

Figure 20. Results of Flow Simulation Within Slit That Models Slip in PCP. (a) Velocity Vector Distribution, (b) Contours of Velocity for Same Dominion.

Increasing the number of elements or nodes produced an increasing number of equations to be solved, which required a greater RAM. A similar result was obtained by readjusting the mesh.

This result demonstrates that these finite element techniques are not suitable for simulating the hydrodynamics of the pump. In general this technique requires a greater number of elements that are transformed in systems of equations that require a computer power beyond what is commonly available. Techniques such as finite volume analysis offer a solution to this problem; nevertheless, the present computer codes for such analysis have limited options with respect to the readjustment of the mesh and the definition of moving boundaries.

EXPERIMENTAL PHENOMENOLOGY

Test Facilities

Test facilities were provided that controlled and registered the main variables of the PCP pumping process; namely, suction pressure, discharge pressure, differential pressure, liquid flow, gas flow, suction temperature, and discharge temperature. Figure 21 shows a scheme of the bench test used in this research.

Liquid was contained in two tanks, and it was supplied to the PCP suction port by an auxiliary pump. A Coriolis flow meter was used to measure the liquid flow, and a heat exchanger was used to hold the temperature of the fluid at 22°C (72°F). A compressor supplied air used in two-phase experiments. The air quantity was measured using a calibrated orifice plate. The pump used was a

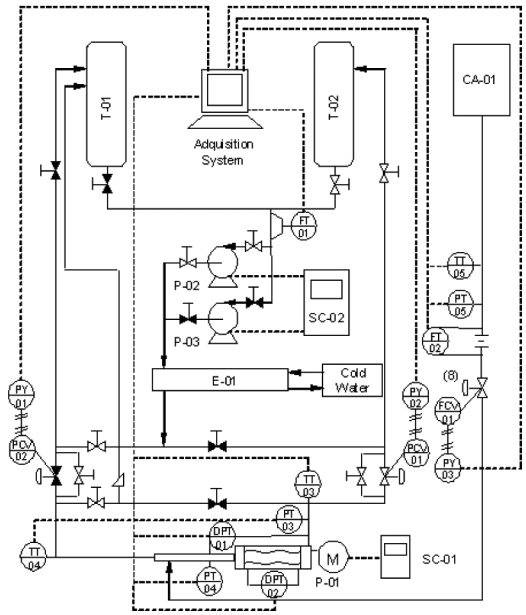

Figure 21. Bench Test Setup.

commercial progressing cavity pump with metallic stator. The geometric parameters were presented earlier in Table 1.

Single-phase testing was conducted using water and three lube oils whose physical properties are shown in Table 2. Lube oil #1 was used as the liquid phase during two-phase experiments.

Pressure sensors were installed inside the pump for measuring the instantaneous pressure distribution as a function of pump shaft position. Figure 22 shows a representation of the PCP with the location of the pressure sensors. For placing these sensors, holes were opened in five sections along the stator. Beginning from the suction port, these sections were separated by a distance equal to the rotor pitch.

Table 2. Characteristics of Liquids Used.

Properties	Lube Oil #1	Lube Oil #2	Lube Oil #3
API	*31.52*	*30*	28
Specific Gravity	0.868	0.878	0.885
Kinematic Viscosity @ 20 ºC (cSt)	20.2	153	545
Kinematic Viscosity @ 100 ºC (cSt)	4.15	6.83	14.43
Dynamic Viscosity @ 20 ºC (cP)		134	481
Dynamic Viscosity @ 100 ºC (cP)		5.66	12

The pressure sensors used can register changes of pressure at a frequency of 1 kHz. The rotor position was inferred from the pump shaft position system, which used an optical key that detected the passage of a flange fixed to the pump shaft.

Experimental Program

Characteristic curves of capacity (Q_{LIQ}) versus differential pressure (ΔP) with single-phase flow were obtained as established

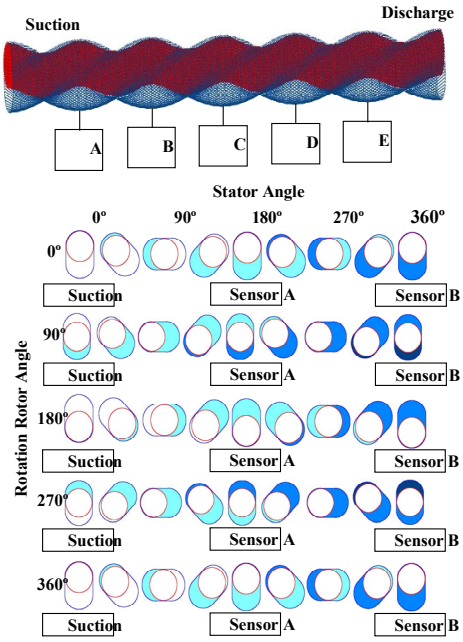

Figure 22. Location of Pressure Sensors Inside PCP.

in the "American National Standard for Rotary Pump Tests" (ANSI/HI 3.6, 1994) and International Organization for Standardization 15136.1 (ISO 15136.1, 2001). For multiphase pumping tests on rotary positive displacement pumps, while a standard does not exist, previous studies (Vetter and Wincek, 1993) in multiphase pumping have probed different procedures to obtain a characteristic curve for two-phase flow; the procedure depending on the experimental facility.

The procedure used here to obtain characteristic curves of total capacity (Q_T) versus differential pressure (ΔP) with two-phase flow consists of obtaining operating points at different speeds of operation at fixed differential pressures, for a total capacity and gas void fraction defined initially (Figure 23).

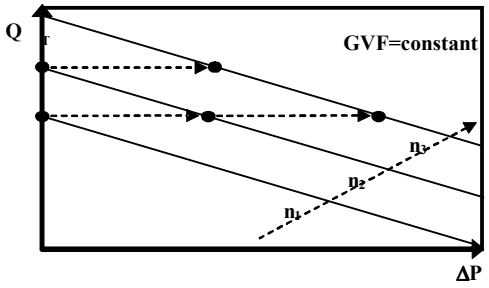

Figure 23. Scheme of Test with Two-Phase Flow.

Total capacity was calculated as the sum of the liquid flow plus the gas flow measured at suction conditions. The gas void fraction at suction conditions was calculated as indicated in Equation (8).

$$GVF = \frac{Q_{GAS}}{Q_{GAS} + Q_{LIQ}} \tag{8}$$

Single Phase-Flow Curves

Figure 24 and Figure 25 present characteristic curves (Q versus ΔP) for a range of liquid viscosity from 1 cP to 480 cP. Both figures show that increasing the differential pressure applied to the pump produces a reduction in flow rate of the liquid. This relationship between differential pressure and flow rate is linear for liquids of high viscosity (above 40 cP), while for liquids of low viscosity

(1 cP) the relationship is nonlinear. This difference in curve shape can be caused by a change in flow regime of the internal slippage that needs to be demonstrated in future studies.

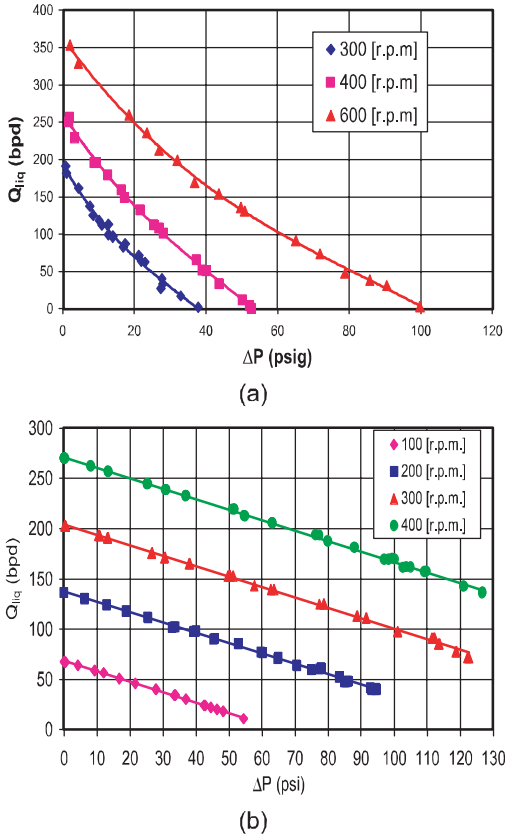

Figure 24. Characteristic Curves of Q Versus ΔP. (a) 1 CP, (b) 42 CP.

The increase of viscosity also produced a greater flow rate. For example, at 300 rpm and ΔP = 38 psi, the flow rate for a 1 cP was 1 BPD (nearly the zero-flow condition), while this flow rate at 480 cP was 220 BPD. The corresponding volumetric efficiency was 0.4 percent for a liquid of 1 cP and 96 percent for a liquid of 480 cP. Another consequence of viscosity was greater differential pressure at which the zero-flow condition occurred. For a liquid of 1 cP, this was reached at ΔP = 40 psi, while for the higher viscosities, it was above 100 psi.

An important experimental observation is that characteristic curves for the low viscosity (1 cP) fluid can be reported only for 300 rpm and above. At 100 and 200 rpm, the zero-flow condition was reached at 5 psig of differential pressure. This differs greatly from the behavior of PCPs with elastomeric stators, implying that PCPs with metallic stators have a minimum speed of operation that depends on the liquid viscosity.

Not only do the results obtained demonstrate that the characteristic curve of a PCP with a metallic stator differs totally from the traditional curve of the PCP with an elastomeric stator material, but it is also possible to conclude that there is some relationship between the mechanical properties of the material and the hydraulic behavior of the pump.

Two-Phase Flow Curves

Figure 26 shows characteristic curves (Q_T versus ΔP) at 400 rpm for a GVF of 0, 20, and 50 percent. The first observation is that Q_T decreases with the increase of ΔP, but does not do it linearly as in the case of single-phase flow. The curves of two-phase flow and the curve of single-phase flow begin from the same value of capacity

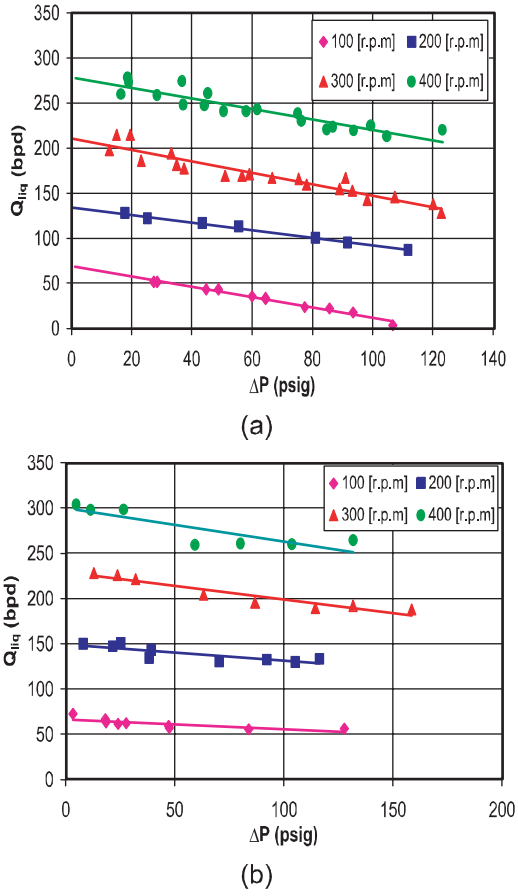

Figure 25. Characteristic Curves of Q Versus ΔP. (a) 34 CP, (b) 480 CP.

(268 BPD) at ΔP = 0 psi. Until reaching certain limiting values of differential pressure (ΔP), the curves of two-phase flow experience an increase in total flow rate (Q_T) with respect to the values that were obtained for the single-phase conditions. This increase was greater for a GVF = 50 percent.

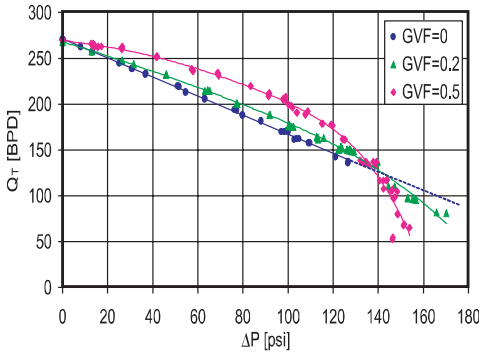

Figure 26. Characteristic Curves with Two-Phase Flow at 400 RPM.

For example, when pump capacity with GVF = 0 is 170 BPD at ΔP = 100 psi, the capacity with GVF = 20 percent is 177 BPD and the capacity with GVF = 50 percent is 199 BPD. For the curves with two-phase flow, a zone develops where the improvement with respect to the single-phase curve begins to decline. If the curve with single-phase flow is extended (refer to dashed line in Figure 26) out to the values of ΔP reached in the tests with two-phase flow, the curves with two-phase flow cut the curve with single-phase flow. In this zone the total capacity with GVF = 50 percent falls faster than the total capacity with GVF = 20 percent.

The behavior observed at 400 rpm is repeated in curves at 300 rpm (Figure 27). In this case, the points where the curves with two-phase flow cut the curve with single-phase flow are within the range of ΔP obtained in the tests. Figure 28 showed curves at 200 rpm; at this speed of operation the increase in the total flow rate with two-phase flow was not observed.

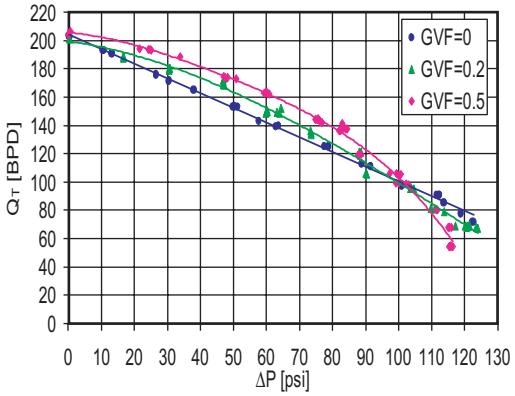

Figure 27. Characteristic Curves with Two-Phase Flow at 300 RPM.

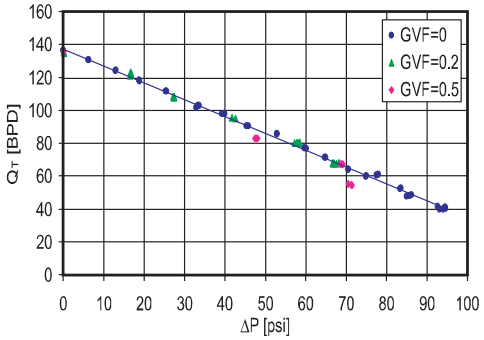

Figure 28. Characteristic Curves with Two-Phase Flow at 200 RPM.

The behavior of the pump for high gas void fractions was studied to try constructing curves with GVF = 80 percent. Nevertheless, for this condition, it was very difficult to reach a stable operating condition (a surging zone was observed). Three points were obtained successfully, one at 300 rpm and the other two at 400 rpm. These points are compared with the single-phase test results in Figure 29.

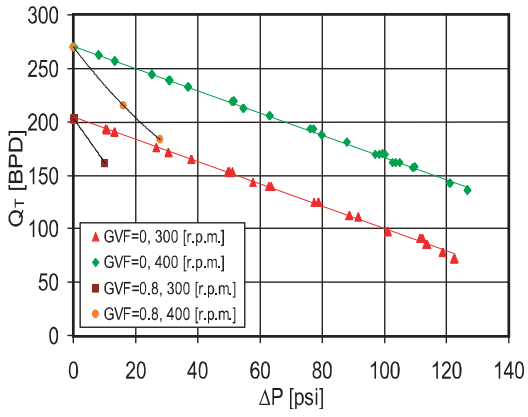

Figure 29. Points of Operation with GVF = 80 Percent.

At 300 rpm and ΔP = 10 psi, the flow rate with single-phase flow is 192 BPD, while the total flow rate with GVF = 80 percent is 162 BPD, which is equivalent to a reduction of 16 percent. At 400 rpm and GVF = 80 percent, the capacity at ΔP = 16 psi is 216 BPD, whereas at ΔP = 28 psi it is 183 BPD. For these same ΔP values, the flow rate with single-phase flow is 254 and 242 BPD, which means that there was a diminution in the capacity of the pump of 15 and 24 percent, respectively, when increasing the GVF up to 80 percent.

For GVF above 20 percent, it is possible to observe two regions of operation. First is the region called "low pressure," which covers the range from zero up to a certain value ΔP, and in this range the total flow rate under two-phase conditions is above that of the single-phase condition. The second region starts with a further increase of the differential pressure, and within it the total flow rate under two-phase conditions is less than single-phase. This is called the "high pressure" region.

Egashira, et al. (1996), Vetter and Wincek (1993), Vetter, et al. (2000), and Yamashita, et al. (2001), have documented better volumetric efficiency when handling gas-liquid mixtures in twin-screw pumps. According to this previous work, a logical assumption could be that for the "low pressure" region the internal slip is principally liquid. It means that the gas phase is not flowing through clearance of the pump. On the other hand this phase is trapped in the cavity, and as it moves with the cavity the gas is compressed. Since part of the energy transfer to fluid is used in compression work, the slippage is reduced.

Nevertheless, by further increasing the differential pressure, some gas could be dragged through clearance. Then all the leaking fluid could be converted into a gas-liquid mixture. Then the slip would have lower apparent viscosity than liquid and would be highly compressible. Therefore, above a given ΔP the slip under two-phase conditions is higher than for the single-phase condition.

This assumption is supported by the observations made of the instantaneous pressure profiles shown in Figure 30 and Figure 31. Here the increase of the GVF diminishes the size of the pressure spikes associated with sealing lines within the pump.

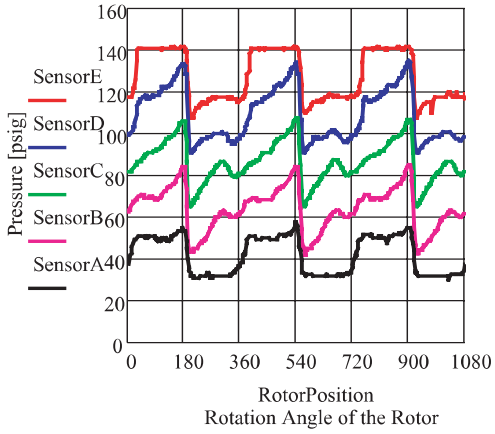

Figure 30. Pressure Profiles at 400 RPM, GVF = 0 Percent, and ΔP = 119.82 PSIG.

Summarizing, within the ranges of operating conditions covered in this study, gas void fraction and speed of operation are the operating variables that affect the performance of the PCP with a metallic stator with two-phase flow. When GVF at the suction is increased, the total flow rate increases and, as a consequence, the volumetric efficiency. This improvement tends to diminish and even to disappear for high values of differential pressure. The volumetric efficiency also increases when the rotational speed is increased and diminishes remarkably with high gas void fractions.

Instantaneous Pressure Profiles

Figure 32 shows instantaneous pressure versus rotor position at 400 rpm, GVF = 0, and ΔP = 119.82 psi. The shape of instantaneous

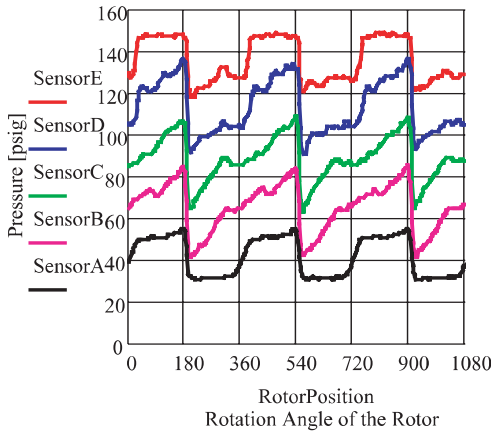

Figure 31. Pressure Profiles at 400 RPM, GVF = 20 Percent, and ΔP = 113.46 PSIG.

pressure registered is repeated in each turn. In this figure it is observed that the shape of the pressure profiles for Sensors A and E are similar to each other, and the same similarity exists among the pressure profiles for Sensors B, C, and D.

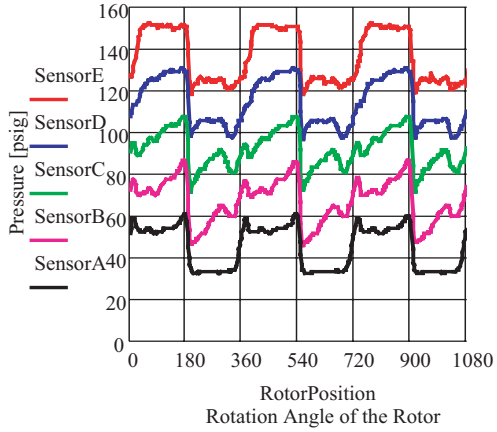

Figure 32. Pressure Profiles at 400 RPM, GVF = 50 Percent, and ΔP = 113.40 PSI.

With the help of Figure 22, it is possible to see that Sensors B, C, and D are always measuring the pressure of cavities that are never completely closed or open to suction and discharge ports. In these cavities the increase of pressure observed in the pressure profiles is due to internal slip. Sensors A and E register the pressure in cavities that are open or close to suction and discharge ports, respectively. Therefore, pressure profiles of these sensors have a stepped form.

At 180 degrees, the rotor is right upon the sensors, and they measure the pressure of sealing lines passing over them. At this point Sensors A and B register pressure spikes. Belcher (1991) observed pressure spikes for an elastomer-stator PCP and explained them comparing the fluid film between the rotor and the stator with a convergent-divergent bearing.

The presence of these pressure spikes also agrees with the results of simulations made for simplified models of a PCP with a metallic stator. It explains the increase of pressure in the clearance as being due to the fluid stagnation that takes place when the fluid pushed by the rotor encounters the fluid leaking through the clearance, and which is the product of the differential pressures between contiguous cavities.

For the five sensors a sudden fall in pressure is observed after 180 degrees, because immediately after the rotor passes over the sensors, they begin to measure the pressure of the previous cavity that has a smaller pressure. Figure 30 and Figure 31 show pressure profiles for GVF = 0.2 and GVF = 0.5 at 400 rpm and ΔP = 113.40 psi. Two observations can be made regarding the causes of these results:

- The increase of GVF produces a diminution in the size of the pressure spikes that occur at 180 degrees, 540 degrees, and 900 degrees; this diminution indicating the presence of gas in the slip flow;
- When GVF increases, the pressure changes inside the pump become smoother (Figure 33).

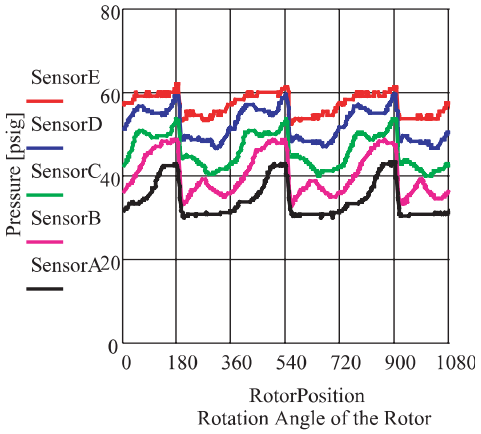

Figure 33. Pressure Profiles at 400 RPM, GVF = 80 Percent, and ΔP = 28 PSI.

Around 360 degrees, the first cavity is close to suction and discharge. When the rotor reaches this position under single-phase conditions, the internal pressure measured by Sensor A increases instantaneously due to the entrapment of the liquid (Figure 34). This position was called the "close point." Later, the rotor continued its movement while pressure inside the cavity was 80 percent greater than suction pressure.

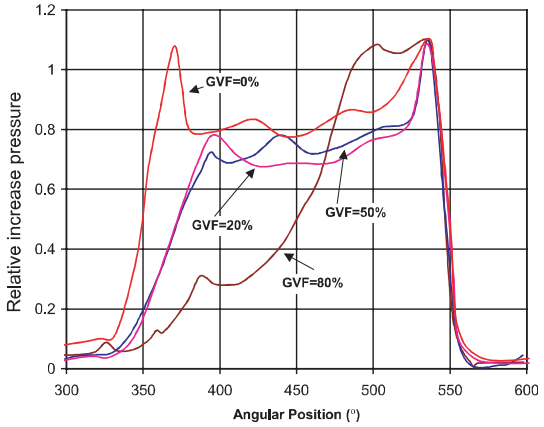

Figure 34. Gas Effect on Instantaneous Pressure of First Cavity at 300 RPM and DP = 28 PSIG.

In the cases of two-phase flow, the increase of pressure does not occur at 360 degrees. For GVF = 20 and 40 percent, the "close point" happened at 390 degrees, and the pressure inside the cavity was 60 percent greater than the suction pressure. Although the "close point" occurred in the same position for a GVF = 80 percent, the pressure reached at this instant was hardly 30 percent greater than the suction pressure.

For the instantaneous pressure profile for GVF = 80 percent, it was observed that after the "close point," approximately 120 degrees of angular displacement is invested in the work of compression, which is not observed in the profiles of 20 and 40 percent.

$$\text{Relative Increase Pressure} = \frac{\left(P_i - P_{suction}\right)}{P_{suction}} \quad (9)$$

Summarizing, the results obtained allow one to conclude that the extreme cavities (suction and discharge) differ in behavior from the rest of the internal cavities. In addition, the instantaneous profiles of the first cavity demonstrate that it plays a fundamental role when the pump handles gas-liquid mixtures. Specifically, this cavity functions to reduce the fraction of gas in the mixture handled in order that the other cavities do not invest their work in compression. When other cavities (in addition to the suction) perform the work of compression (as in the case of GVF = 80 percent), the pump operates less efficiently and total flow rate drops quickly at low differential pressure.

CONCLUSIONS

The analytical and experimental research results reported in this paper have validated the concept of utilizing a metallic stator in a progressive cavity pump. Even though this necessitates introducing a clearance between the rotor and stator and the attendant internal leakage or slip, the extensive experimental results reported herein confirm the ability of this new PCP to handle single- and two-phase fluids with reasonable volumetric efficiency. The tests were conducted on a PCP with a 40 mm (1.58 inch) diameter rotor over a range of rotative speed, mainly from 200 to 400 rpm. The pump pressure rise in the experiments reached 170 psi (1.17 MPa) in two-phase flow for which the viscosity of the liquid phase was 42 cP and the gas void fraction was 20 percent. At 80 percent GVF, the pressure rise reached 130 psi (0.9 MPa).

The computed results from three different models for simulating flow in this PCP were compared with the test results and provided further insights, described as follows:

• The results obtained for the "infinite parallel plate" model indicate that the sealing within a PCP without interference is due as much to the rotation of the rotor as it is to the differential pressure between the cavities. Besides, they indicate that the hydraulic mechanism of sealing in a PCP is characterized by zones of "concurrence" and "recirculation" (or of "inhibition" and "augmentation") of the flow in the clearance between the rotor and the stator.

• Simulation via the "2D untwisted (developed) model" demonstrates that the slippage between the cavities must be understood as a zone of stagnation where the relative velocity of the fluid with respect to the rotor is reduced. It produces a reduction of the instantaneous volume displaced by the machine when a differential pressure is applied.

• The finite element techniques employed cannot solve the "real model of a PCP." Moreover, the results led to the conclusion that finite element analysis (FEA) techniques are not readily adapted for simulating the hydrodynamics of this kind of pump. In general this technique requires a large number of elements that are transformed into systems of equations that require more than standard computing power. Techniques such as the finite volume method offer a solution to this problem; nevertheless, present codes have limited options for readjustment of the mesh and for handling variable boundaries.

The experimental results revealed the following operational characteristics of the PCP with the metallic stator, some of which are supported by the above simulations:

• The flow rate of the pump under single-phase flow conditions increases with increasing speed of operation and liquid viscosity, but diminishes with differential pressure. This agrees with the result of simulation via the "untwisted model."

• The performance in two-phase flow depends mainly on the gas content in the pump and on its speed of operation. Within a limited range of differential pressure, the increase of GVF produced a greater total flow rate than the single-phase condition. Nevertheless, this improvement tends to disappear when the differential pressure is raised.

• Instantaneous pressure profiles based on the rotor position were obtained and were used to study the internal operation of the pump. This enabled observation of the behavior of slip versus differential pressure and GVF. A proposed hypothesis of behavior under two-phase conditions is that there exists a range of differential pressure where the slip flow is predominantly liquid, but an increase of differential pressure beyond this range initiates dragging of gas bubbles into the clearances, requiring that the slip be treated as a liquid-gas mixture.

• The presence of spikes in measured instantaneous pressure profiles accords with the results of simulations made for simplified models of a PCP with a metallic stator.

NOMENCLATURE

w	=	Interference
d_r	=	Rotor diameter
d_{st}	=	Stator diameter
A	=	Area
e	=	Eccentricity
$Paso_{st}$	=	Stator pitch
$Pitch_{st}$	=	Stator pitch
D	=	Displacement
n_{rotor}	=	Operation speed
u_x, u_y, u_z	=	Fluid velocity
P_x, P_y	=	Port pressure
U_T	=	Tangential velocity
n	=	Operation speed
h	=	Height cavity
ϕ_{st}	=	Angle of one point in transversal section of stator
ϕ_r	=	Angle of one point in transversal section of rotor
α_{st}	=	Stator helix angle
R_l	=	Modulus of transversal section geometry
i, j, k	=	Axes index
U_n	=	Axial velocity
ω	=	Angular speed
Q_{liq}	=	Liquid flow rate
Q_T	=	Total flow rate
ΔP	=	Differential pressure
GVF	=	Gas void fraction
P_i	=	Instantaneous pressure
$P_{suction}$	=	Suction pressure
FEA	=	Finite element analysis
Q_{GAS}	=	*In situ* gas flow rate

REFERENCES

ANSI/HI 3.6, 1994, "American National Standard for Rotary Pump Tests," Hydraulic Institute, Parsippany, New Jersey.

Arrellano, J. A., 1998, *Field Study for Predicting PC Pump Performance*, Tulsa, Oklahoma: Society of Petroleum Engineers.

Belcher, I., 1991, "An Investigation into the Operating Characteristics of the Progressive Cavity Pump," Doctoral Thesis at The British Library, United Kingdom.

Cholet, H., 1997, *Progressing Cavity Pumps*, Paris, France: Éditions Technip.

Cooper, P., Heald, C., Karassik, I., and Messina, J., 2001, *Pump Handbook*, Third Edition, New York, New York: McGraw Hill.

Cooper, P., Schiavello, B., de Marolles, C., de Salis, J., Prang, A. J., and Broussard, D. H., 1996, "Multiphase Gas-Liquid

Pumping," *Proceedings of the Thirteenth International Pump Users Symposium*, Turbomachinery Laboratory, Texas A&M University, College Station, Texas, pp. 159-174.

Dillon, M. and Vullings, K., 1999, "Applying the NPSHR Standard to Progressing Cavity Pumps," *Pumps & Systems Magazine*.

Dunn, L., Matthews, C., and Zahacy, T., 1994, "Progressing Cavity Pumping Systems: Design, Operation and Performance Optimization," Course Manual, Centre for Frontier Engineering Research (C-Fer), Alberta, Canada.

Egashira, K., Shoda, S., and Tochikawa, T., October, 1996, "Backflow in Twin-Screw-Type Multiphase Pump," SPE 36596, Paper Presented at the SPE Annual Technical Conference, Denver, Colorado.

Gamboa, J., 2000, "Simulation Computational de una BCP Sin Interferencia," Master Thesis, Universidad Simón Bolívar, Sartenejas, Venezuela.

Gómez, B., 2000, "Modelo Analítico para la estimación del NPSH requerido para Bombas de Cavidades," Bachelor Thesis, Universidad Simón Bolívar, Sartenejas, Venezuela.

Huebner, K. and Thornton, E., 1982, *The Finite Element Method for Engineers*, Second Edition, New York, New York: John Wiley & Sons.

ISO 15136.1, 2001, "Downhole Equipment for Petroleum and Natural Gas Industries—Progressing Cavity Pump Systems for Artificial Lift—Part 1: Pumps," International Organization for Standardization, Geneva, Switzerland.

Martín, A., December, 1999, "New Approach Describes Multiphase Flow Behavior in Single and Twin-Screw Pumps," TAMU 9974, Paper Presented at the Texas A&M University Student Paper Contest, College Station, Texas.

Martin, A., Kenyery, F., and Tremante, A., 1999, "Experimental Study of Two-Phase Pumping in Progressive Cavity Pumps," Society of Petroleum Engineers, SPE 53967, Caracas, Venezuela.

Moineau, R., 1930, "A New Capsulism," Doctoral Thesis, The University of Paris, Paris, France.

Olivet, A., 2002, "Estudio Experimental del desempeño de una BCP de Estator Rígido con Flujo Bifásico," Master Thesis, Universidad Simón Bolívar, Sartenejas, Venezuela.

Osio, I. and Moreno, N., 1996, "Modelaje y Simulación Numérica de Bombas de Cavidades Progresivas," Technical Report, PDVSA Intevep S.A. Los Teques, Venezuela.

Pardey, R., 1999, "Evaluación de Elastomeros para BCP," Technical Report, PDVSA Intevep S.A. Los Teques, Venezuela.

Robles, J. and Ercolino, J., 1986, "Analisis de Fuerzas Internas en Bombas de Cavidades Progresivas," Internal Technical Report, PDVSA-Intevep, Los Teques, Venezuela.

Robles, J. and Moreno, N., 1995, "Modelaje y Simulación Númerica de una BCP- Analisis Hidrodinámico," Internal Technical Report, PDVSA-Intevep, Los Teques, Venezuela.

Schlichting, H., 1986, *Boundary Layer Theory*, Seventh Edition, New York, New York: McGraw-Hill.

Vetter, G. and Paluchowski, D., 1997, "Modeling of NPSHR for Progressing Cavity Pumps," ASME Fluids Engineering Division Summer Meeting, Vancouver, British Columbia.

Vetter, G. and Wincek, M., 1993, "Performance Prediction of Twin Screw Pumps for Two-Phase Gas/Liquid Flow," *Pumping Machinery*, Edited by Paul Cooper, ASME FED Volume 154.

Vetter, G. and Wirth, W., 1995, "Understand Progressing Cavity Pumps Characteristics and Avoid Abrasive Wear," *Proceedings of the Twelfth International Pump Users Symposium*, Turbomachinery Laboratory, Texas A&M University, College Station, Texas, pp. 47-60.

Vetter, G., Wirth, W., Körner, H., and Pregler, S., 2000, "Multiphase Pumping with Twin-Screw Pumps—Understand and Model Hydrodynamics and Hydroabrasive Wear," *Proceedings of the Seventeenth International Pump Users Symposium*, Turbomachinery Laboratory, Texas A&M University, College Station, Texas, pp. 153-170.

Yamashita, M., Sharma, Y., and Ihara, M., March 2001, "Pre-Field Trial Testing of a Twin Screw Multiphase Pump," SPE 68223, Paper Presented at the SPE Middle East Oil Show, Bahrain.